CrystEngComm

Accepted Manuscript

ROYAL SOCIETY OF CHEMISTRY

www.rsc.org/crystengcomm

Journal Name

RSCPublishing

ARTICLE

One-Step Synthesis of Near-Infrared Emission and Size Tunable $CuInS_2$ Semiconductor Nanocrystals by Adjusting Kinetic Variables

Chenghui Xia, [a, b] Lixin Cao,[*, b] Wei Liu, [b] Ge Su, [b] Rongjie Gao, [b] Hua Qu, [b] Liang Shi, [a] and Guanghui He [b]

Cite this: DOI: 10.1039/x0xx00000x

Received 00th January 2012,
Accepted 00th January 2012

DOI: 10.1039/x0xx00000x

www.rsc.org/

This paper aimed at systematically optimizing the preparation process of $CuInS_2$ (CIS) QDs by intensively manipulating kinetic variables including reaction temperature, reaction time, In/Cu ratio and surface ligand. CIS QDs were synthesized by copper iodide and indium acetate in the presence of 1-octadecene (ODE) that regarded as reaction solvent, while 1-dodecanethiol (DDT) was chosen as sulfur source and surface ligand. UV-Vis spectrophotometer and fluorescence spectrophotometer were applied to unearth the growth kinetics and fluorescence properties of CIS QDs. Transmission electron microscopy and X-ray diffraction were utilized to characterize the size, morphology and crystal structure of final products. Our results reveal that the emission wavelength of CIS QDs could bridge visible light and near-infrared ranging from 630 to 825nm. By scrupulously regulating reaction temperature, reaction time and amount of DDT, highly dispersed and stable CIS QDs could be prepared without further disposing. The fluorescent intensity could be enhanced by introducing Cu defects with fluorescence quantum yield (QY%) reaching around 7%, while the particle size could be tuned from ultra-small approaching 1.5nm to 4nm by controlling In/Cu ratio.

Introduction

Semiconductor quantum dots (QDs) refer to semiconductor nanocrystals, which are widely used in bioimaging,[1-2] solar cells[3-5] and light-emitting diodes[6-7] because of their unique electric and optical properties. Semiconductor QDs are mainly divided by the position of components in the periodic table of elements, for instance, the II – VI (CdS, CdSe, CdTe, ZnO, ZnS, ZnSe, ZnTe),[8-10] III – V (InP, InAs, GaN, GaP, GaAs),[11-12] IV – VI (PbS, PbSe, PbTe),[13-14] and the ternary compound Ⅰ-Ⅲ-Ⅵ ($CuInS_2$, $CuInSe_2$, $AgInS_2$, $AgInSe_2$).[15-18] CdX (X=S, Se, Te) QDs are especially attractive due to the wide range of emission color which spans from ultraviolet to near-infrared,[19] while PbX QDs can be engineered to absorb and emit in a vast spectral range, spanning from 800 to 4000 nm with high fluorescence quantum yield (QY%).[20] Unfortunately, these kinds of QDs possess an inextricable defect i.e. high toxicity that severely limits their possible applications. In order to combat this issue, a potential alternative material, being more benign and less toxic, but having a tunable photoluminescence emission wavelength from visible to near-infrared range, is cooper indium sulfur (CIS) with a direct band gap of 1.5eV in bulk status[21] and excitation Bohr radius of 4.1nm[22]. Additionally, as biological tissues scatter and absorb less light and low auto-fluorescence at longer wavelengths, the near-infrared emission wavelength can more efficiently penetrate skin and blood than visible light.[23-24] For these outstanding properties, CIS QDs are doomed to be extraordinary promising materials applied to biological areas e.g. fluorescent contrast agent in vivo.[2]

Previous papers have reported a variety of methods like pyrolysis of molecular single-source precursors,[22, 25-26] hot-injection method[27-28] and solvothermal method[29-30] to prepare CIS nanoparticles. However, few of them were directly applied to synthesize high quality products without further disposing and it is still a big challenge to realize a repeatable production on large scale. Castro and coworkers[25] firstly reported the synthesis of ternary chalcopyrite CIS nanoparticles by thermal decomposition of single-source precursor $(PPh_3)_2CuIn(SEt)_4$. This method was limited by the precursor's availability and their tedious complicated synthesis procedure, although they claimed that the average size of CIS could range from 2 to 4nm with the fluorescence quantum yield of 4.4 %. In addition, due to the maturity of hot-injection technique used in preparing CdX, many scientists imitated this method to prepare CIS QDs. Maeda et al.[31] demonstrated control of optical properties, band-gap energy, and photoluminescence emission wavelength through alloying processes of chalcopyrite ZnCuInS (ZCIS) with QY% of 5 % and emission wavelength tuning within 550-800nm by hot-injection method. Because of rigorous reaction conditions, expensive raw materials and complex synthesis processes, it is not a cost efficient strategy to employ hot-inject method in the preparation of Ⅰ-Ⅲ-Ⅵ QDs. As researchers continue to push the envelope, they are looking for new

approaches to prepare ideal CIS QDs. In recent years, Reiss et al.[32] and Klimov et al.[16] almost simultaneously provided a simple and reliable synthesis method for CIS/ZnS core-shell Ⅰ-type semiconductor QDs showing increased QY% and high photostability. This kind of new technique, namely, one-pot method is conducted by adding all reaction precursors into a three-necked flask and achieving the final products by adjusting proper reaction temperature. Because of the simple synthesis process, high repeatability and large-scale capability, one-pot method is flourishing quickly and widely in preparing CIS and other Ⅰ-Ⅲ-Ⅵ QDs[33]. In spite of the attractive superiorities, one-pot technique is not mature enough and the technical process needs to be optimized to prepare CIS QDs with outstanding crystallinity and fluorescence stability.

In this paper, we directly adopted one-pot method, using CuI, $In(Ac)_3$, 1-dodecanethiol (DDT) and 1-octadecene (ODE) as precursor, to simply synthesize remarkable stable and monodispersity bare CIS QDs with photoluminescence ability ranging from 630 to 825 nm by meticulously adjusting kinetic variables including reaction temperature, reaction time, cationic ratio and surface ligands. Furthermore, the nucleation, grain growth and possible formation mechanism of CIS QDs were analysed and inferred indirectly. By controlling In/Cu ratio, the QY% had been enhanced to 7% and the size could be tuned from 1.5 to 4nm. Compared with previous reports, we are more systematic and straightforward to investigate the influence of reaction conditions on the preparation of near-infrared emission CIS QDs, which paves a solid foundation for the future synthesis of Ⅰ-Ⅲ-Ⅵ QDs.

Experimental

Materials

Indium (III) acetate ($In(OAc)_3$, 99.99%) was purchased from Sigma-Aldrich. Copper(I) iodide (99.95%), 1-dodecanethiol (DDT, 98%), 1-octadecene (ODE, 90%) were bought from Aladdin Reagent and all other products were purchased from Sinopharm Chemical Reagent Beijing Co., Ltd. All reagents were used without further purification.

Preparation of CIS QDs

CIS QDs were synthesized according to the method reported previously.[18, 32, 33] Briefly, CuI (0.0190g, 0.1mmol) and $In(Ac)_3$ (0.0292g, 0.1mmol) were mixed with 2.00 ml of DDT in the presence of 10.00 ml ODE in a 100ml three-necked flask equipped with a condenser, thermometer, and magnetic stirring. The mixed solution was degassed at room temperature for half an hour and purified by flowing argon. When the bubbling subsided, the temperature was increased to 80℃ and ditto degassed. Subsequently, under a flow of purified argon, the system was heated at 120℃ until a clear solution could be observed. Finally, the temperature was boosted to 230 ℃ (180-250℃), and the color of the solution changed progressively from colorless to slightly yellow, red, dark and finally black. During this process, sampling should be accomplished at fixed time intervals and the crude products were dispersed in hexane, precipitated by adding an excess of acetone, and centrifuging or decanting. The QDs required to be redispersed in hexane after precipitation/dispersion cycle sustained at least twice to eliminate byproducts and unreacted precursors. The purified products were used for measurement of optical characterization, e.g., UV-vis absorption spectra and photoluminescence spectra.

Characterization

Powder X-ray diffraction (XRD) patterns were obtained on a BRUKER D8 ADVANCE X-ray diffractometer fitted with Cu Kα radiation over the 2θ range from 20° to 70°, and the scanning speed was 4°/min. Fourier transform infrared spectrum (FT-IR) was recorded by Nicolet 6700 Fourier transform infrared spectrometer over the range from 400 nm to 4000 nm. The powder samples were prepared by drying the purified products under vacuum at 60℃ for 20 hours. Transmission electron microscopy (TEM) images were carried out on a JEOL JEM-1200EX transmission electron microscope at an acceleration voltage of 200 kV, while high resolution transmission electron microscopy (HRTEM) and energy dispersive spectrometer (EDS) data were collected by JEOL JEM-2100 transmission electron microscope. Samples for TEM and EDS measurement were prepared by depositing one drop of diluted hexane solution products on a carbon-coated copper/nickel grid and drying at room temperature. The samples' particle sizes were measured by nano-measurer from TEM micrographs, and corresponding size distribution histograms were obtained based on the statistics of measurement results. Then Gauss curve fitting should be accomplished to reduce the measurement error. UV-vis absorption spectra and photoluminescence spectra were achieved on Shimadzu UV-2550 spectrophotometer and HORIBA Jobin Yvon FluoroLog3-p fluorescence spectrophotometer at room temperature, respectively. Solutions were injected into 10mm quartz cuvette for optical measurement. In more detail, the photoluminescence emission (PL) spectra were obtained with the excitation wavelength at 470nm. Fluorescence quantum yeild (QY%) measurements refer to ref [32]. The QY% of samples were determined by comparison of the integrated fluorescence intensity of CIS QDs' dispersion in hexane with that of a standard organic dye i.e. Rhodamine 6G (QY%=95%) in ethanol, whose PL spectrum overlaps significantly with that of the nanocrystal sample under the same setting of FluoroLog3-p fluorescence spectrophotometer. The absorbance of all solutions was maintained below 0.1 au at 488nm (excitation wavelength for the measurement of QY%) to avoid internal filter effects. Each sample was determined for at least three different concentrations to ensure the accuracy of determinand's QY%. The fluorescent digital pictures of CIS QDs dispersed in hexane were taken in ZF-7 Ultraviolet Analyzer at 365 nm UV lamp excitation.

Results and discussion

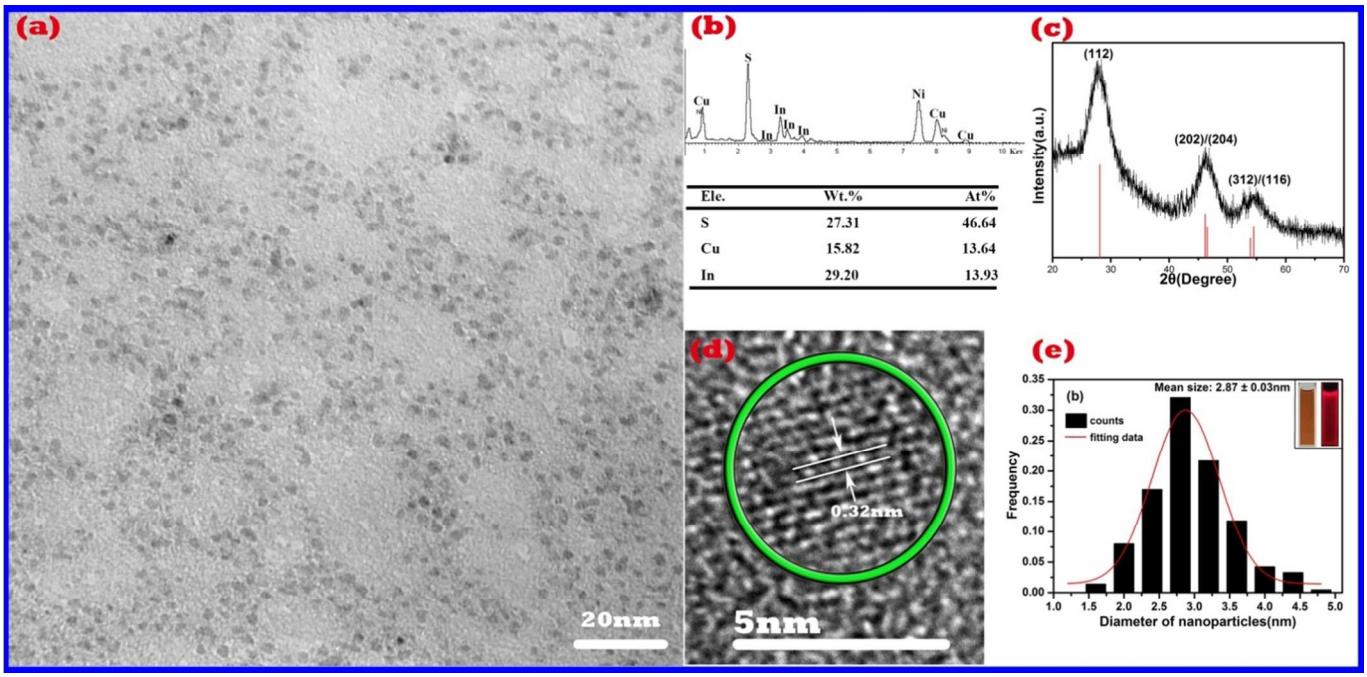

Fig.1 The structure and morphology of CIS QDs extracting at 30min prepared at 230 ℃. (a) TEM image of CIS QDs; (b) EDS patterns of CIS QDs; (c) XRD pattern of CIS QDs; (d) HRTEM image of CIS QDs; (e) Particle size distribution of CIS QDs obtained by nano-measurer estimated from fig. 1a with a inset of natural color and fluorescent digital pictures excited at 365nm by UV lamp.

The kinetic variables and surface ligand have a great influence on the crystal growth processes, microstructure and optical properties of CIS QDs. By an intensive investigation on the reaction conditions, high quality QDs can be prepared with a fine repeatability. Meanwhile, it lays a solid foundation for the in-depth study of the crystal nucleation and growth, which guides us forward deducing and understanding the formation mechanism of ternary CIS QDs.

Structure and morphology characterization

The crystalline phase of CIS QDs mainly includes chalcopyrite, zinc blende and wurtzite. Commonly, the bulk CIS tends to be chalcopyrite crystal structure at room temperature, whereas zinc blende (1248K) and wurtzite (1313K) are stable only at high temperatures.[34] Theoretically, the phase transformation can be realized by altering the reaction conditions. X-ray powder diffraction was used to characterize the phase structure of as-prepared CIS QDs. As can be seen from fig.1c, the first three relatively distinct broad diffraction peaks (around 28°, 46° and 55°) can be indexed to the (112), (204)/(220), and (312)/(116) reflections of the tetragonal crystal structure. In spite of the tiny difference between chalcopyrite phase and zinc blende phase, the CIS QDs with zinc blende phase usually have a diffraction peak of (200).[33, 35-36] In fig.1c, the absent of this peak can be an evidence for the chalcopyrite phase. The HRTEM image of corresponding nanoparticles is shown in the inset of fig. 1d, where the lattice fringe d=0.32nm corresponds to the (112) lattice plane of tetragonal CIS QDs. Therefore, the nanocrystals prepared by one-pot method are tetragonal chalcopyrite CIS and no other phases are produced in the reaction. Meanwhile, TEM observations were also employed to study the CIS QDs. The TEM image (fig. 1a) demonstrates that the particles exhibit a decent uniform size distribution and irregular nanorod structure. By Gauss curve fitting of particle size measurement results statistics (fig. 1e), the average size of as-prepared samples is 2.87±0.03nm in diameter which is smaller than the exciton Bohr radius i.e. 4.1nm. Besides, EDS patterns (fig.1b) confirm that the cationic mole ratio abides by the stoichiometric ratio, whereas the excessive volume of sulfur probably comes from surface ligand ensuring the high stability of crude products.

The influence of reaction temperature

We systematically investigated the influence of reaction temperature ranging from 180 to 250℃ in order to give a guidance on the synthesis of CIS NCs. Theoretically, boosting reaction temperature can provide the reaction precursors with more energy to be active. The high activity is not only beneficial to the formation of new compounds but also good for the growth of nanocrystals.

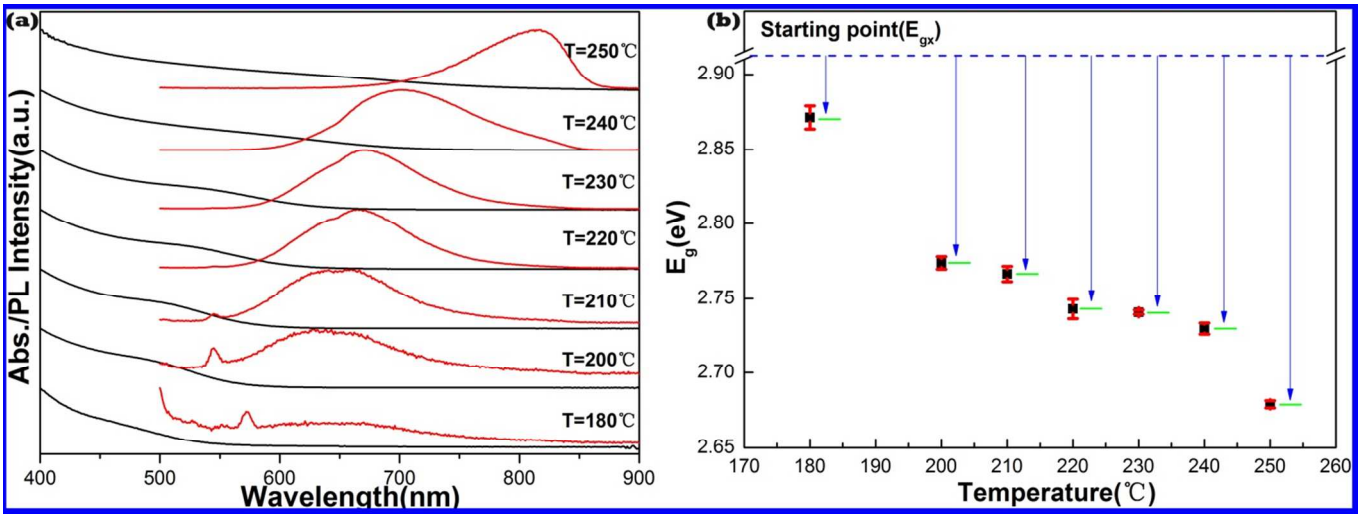

Fig. 2 (a) UV-vis absorption spectra and corresponding PL spectra. (b) E_g calculated by equation 1 in supplementary information. Samples were extracted at 10min under different reaction temperature ranging from 180 to 250℃.

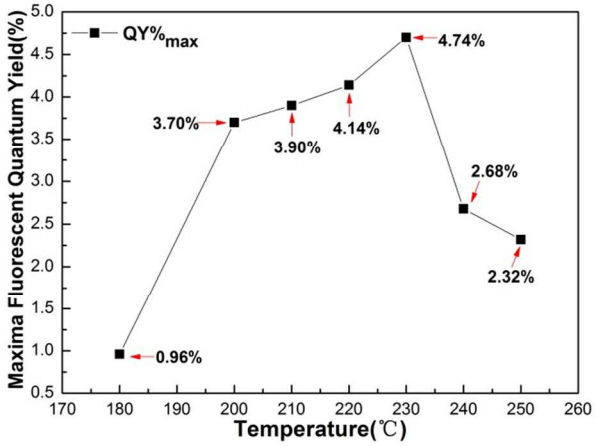

Fig. 3 The maximum QY% of CIS QDs under different reaction temperature ranging from 180 to 250℃

As can be seen from fig. 2a, sampling was accomplished in the initial 10 minutes under each different reaction temperature. When the temperature is 180℃, the growth rate of nanocrystals is low, while the fluorescent intensity is rather week and PL peak position locates around 630nm. Yet, the obvious red shift can be found by boosting reaction temperature gradually. When the temperature reaches 250℃, the emission wavelength peaks at about 815nm and growth speed is substantially enhanced. Things would develop in the opposite direction when the temperature is too high(≥250℃), the excessive decomposition rate or even the damage of the surface ligand structure of CIS QDs will cause the instability of nanocrystals. In fig. 2b, given that the band gap (E_g) of the smallest CIS QDs is E_{gx} (the starting point), which is initially the same, E_g will show difference in a fixed interval because of the difference of nucleation and growth speed under diverse reaction temperature, theoretically. Fig. 2b confirms that the gap (E_g–E_{gx}) get wider along with the enhancement of reaction temperature, which represents the bigger particle size. It gives clear evidence that boosting temperature is beneficial to accelerate the growth of CIS QDs.

Fig.3 shows the QY% experiences an upward trend from 0.96% to 4.7% during the temperature from 180℃ to 230℃. As the temperature consistently increases, a downward trend is easily observed. The decrease of QY% may connect with the decomposition of surface ligand on the CIS QDs. When the temperature is over-enhanced, the severe decomposition of surfaced ligand will reduce the stability of nanocrystals and lead to aggregation of small sized CIS QDs. By contrast, the proper temperature is beneficial both to the generation of sulfur resource and the perfect growth of crystal structure. Therefore, the fluctuation of QY% is reasonable when the temperature changes regularly. Consequently, for purpose of safety, higher fluorescent intensity and good manipuility, 230℃ is a wise choice for preparing high QY% and uniform size of CIS QDs.

The influence of reaction time

In the synthesis process of CIS QDs, the quality of products depends to a large extent on an appropriate reaction time that is closely linked with the nucleation and growth of nanoparticles. When the reaction time is not adequate, the quality of QDs tends to be poor. On the opposite, excessive prolonging the reaction time will induce to the aggregation of small size crystals, which eventually effects on the size distribution and stability of CIS QDs.

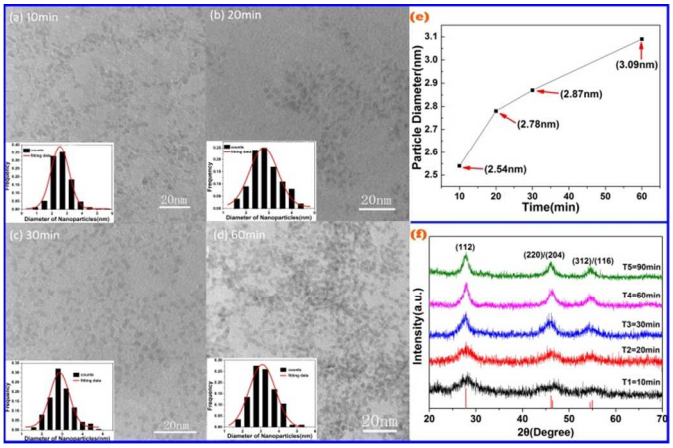

Fig. 4 TEM of CIS QDs isolated at different times at 230℃: (a) 10min, (b) 20min, (c) 30min, (d) 60min. Inset in the up right corner (e) and bottom right corner (f): Corresponding particle diameter and XRD patterns of samples.

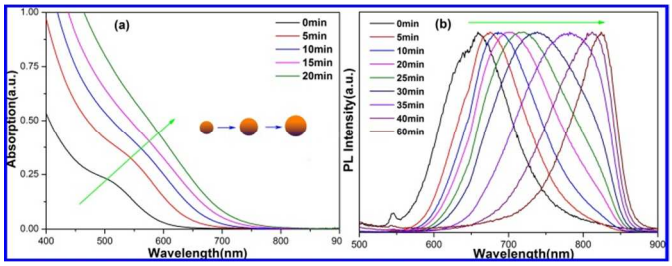

Fig. 5 Optical characterization of CIS QDs under different reaction time at 230℃: (a) UV-vis absorption spectra during the first 20min. (b) PL spectra excited at 470nm during the first 60 mins.

Here, we investigated the influence of reaction time on the crystal growth and optical properties of CIS QDs at 230℃. Sampling was conducted at a fixed time intervals to figure out the changes of CIS particles. Fig. 4f confirms that the crystal structure of CIS QDs maintains stable at chalcopyrite phase and no other phases are produced with the extension of reaction time to 90mins. Before the first 10min, obvious noise can be found owing to the poor crystallinity, and full width at half maximum (FWHM) is quite large because of the ultra-small size. By prolonging reaction time, XRD patterns tends to be more distinct, reduced noise and narrow FWHM, which indicates the better crystalline and larger particle size.

Fig. 5 shows that the UV-vis absorption and PL spectra are both apparent red shift during the 60 minutes respectively, which indirectly proves the particles increasing gradually by extending reaction time. More specifically, it is obvious from fig.5a that the extent of red shift is greater in the first 10min than that after 10min. This phenomenon suggests that the nucleation probably occupies the main status in the first process. Abiding to Oswald ripening principle, once the nucleation finished, the growth of CIS immediately replaces the status of nucleation. Due to larger surface energy of smaller size of CIS, the initial products aggregate to lessen the surface energy. Then, the speed of growth decreases as the crystal structure is perfect and surface energy become lower. Yet, the stability of CIS QDs will sharply descend and congregate to grow into bulk because the surface ligand decomposes with the continuous prolonging of reaction time. It is strong evidence that the well-dispersed CIS colloid will turn into muddy state by lengthening the reaction time. Moreover, Fig. 5(b) indicates that the emission wavelength range from 630nm to approximate 825nm during the period from 0 to 60min, while the maximum emission intensity peaks at around 700nm and QY% is about 4.7%. It is not difficult to find that FWHM of CIS QDs in the PL spectra see an upward trend before the peak position reaching 800nm and then decreases after that. This indicates that the size distribution of nanoparticles is uniform during the nucleation and early stage of crystal growth. Then, owing to Ostwald ripening, the crystal competes to grow and leads to appearance of inhomogenous particles, which coincides with TEM images (fig. 4a-d), thereby, FWHM in PL spectra is large. As the structure of crystal getting perfect and surface energy getting lower, the size of particle tends to be stable and exhibits tiny difference bringing about the reduction of FWHM. TEM images demonstrate that the particles remain nanorod-shaped and grow consistently from 2.54±0.04 to 3.09±0.04 nm during 60mins. Fig. 4e straightforwardly demonstrates the growth rate of CIS QDs is in line with the analysis of UV-vis absorption from fig. 3a. Therefore, the size and emission wavelength of CIS nanocrystals can be tuned by adjusting the reaction time effectively.

The influence of In/Cu molar ratio

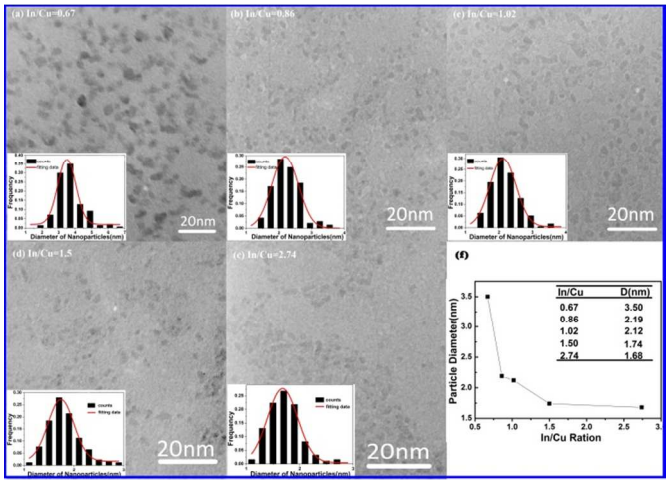

Fig. 6 The structure and morphology of CIS QDs under different In/Cu ratio. (a-e) TEM images and corresponding size distribution histograms inside. (f) Particle diameter.

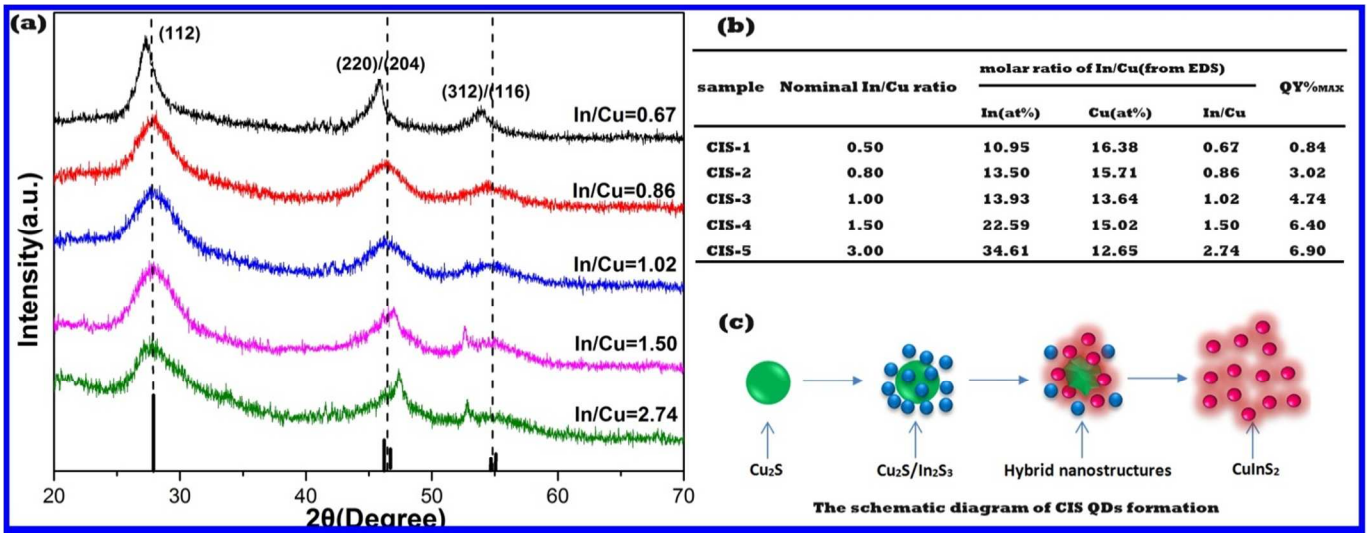

sample	Nominal In/Cu ratio	molar ratio of In/Cu(from EDS)			QY%MAX
		In(at%)	Cu(at%)	In/Cu	
CIS-1	0.50	10.95	16.38	0.67	0.84
CIS-2	0.80	13.50	15.71	0.86	3.02
CIS-3	1.00	13.93	13.64	1.02	4.74
CIS-4	1.50	22.59	15.02	1.50	6.40
CIS-5	3.00	34.61	12.65	2.74	6.90

Fig. 7 (a) XRD patterns of CIS QDs with different In/Cu ratio at 10min under 230℃. (b) Nominal, actual In/Cu ratio and corresponding $QY\%_{max}$. (c) The schematic diagram of CIS QDs formation.

Since CIS QDs are ternary nanoparticles, the component proportion especially the cationic ratio is an important factor in controlling nucleation, grain growth, crystal structure and fluorescent intensity. Previous works reported that the size of CIS QDs was closely related to the cationic ratio.[16, 18, 40] They claimed that along with the increase of indium source, the size of CIS QDs tended to be smaller.[16] Unfortunately, there are few papers to interpret the intrinsic reasons on this issue.

By regulating the amount of CuI and $In(Ac)_3$ precursors (referring to fig.7b), In/Cu molar ratio of the resulting CIS QDs was gradually tuned from 0.5 to 3.0. XRD and TEM were taken at the first 10min with different cationic ratio to characterize the imperceptible structural changes. XRD patterns (Fig.7a) show that three obvious diffraction peaks correspond to the (112), (220)/(204), and (312)/(116) planes of the tetragonal phase, which mirrors that the resulting samples are tetragonal phase, although there are very small amount of measurable secondary phase in some products and slight angular deflection caused by lattice distortion. As the decrease of In/Cu, the FWHM in XRD tends to be narrower which means the smaller particle size. Furthermore, TEM images (fig. 6) further confirm that the average size of CIS QDs at the first 10min decrease from 3.5 to 1.68nm as the increase of In/Cu molar ratio from 0.67 to 2.74 in accordance with analysis of XRD.

Considering the cause of dimensional change, the formation mechanism of CIS QDs shall be clearly understood. Previous works thought that the formation of Cu_2S-$CuInS_2$ hybrid nanostructures was an essential intermediate step in the growth of CIS QDs.[41-44] As can be seen from the fig. 7c, the whole CIS formation process can be divided into three stages. As DDT is soft base, it probably prefers to combine with soft acid i.e. Cu^+, therefore the formation of Cu_2S nanoparticles can be accompanied naturally. Subsequently, DDT reacts with the In^{3+} and form In_2S_3 nanocrystals, which gradually deposit onto and diffuse into the surface of Cu_2S. Eventually, the extraneous In_2S_3 erodes original Cu_2S and forms the CIS QDs. The whole process suggests that the morphology of CIS QDs is determined by the initial matrix i.e. Cu_2S. Moreover, In^{3+} plays a pivotal role like aggressive agent that undermines the original Cu_2S particles and forms ultimate products, namely CIS QDs. Therefore, the high concentration of indium source promotes the formation of pony-size CIS QDs.

Meanwhile, on the basis of previous work[45-47], the fluorescence of CIS QDs originates not from band excition recombination but from donar-acceptor transition (DAT) (sulfur vacancy and copper indium substitution as the donor, and copper vacancy as the acceptor), which is closely linked with the crystal defects, QY% can be enhanced by intentionally introducing the crystal defect, thereby controlling the composition of products. Uehara et al.[48] suggested that Cu deficient could directly relate to CIS QDs' crystal defects. In more detail, in chalcopyrite CIS QDs, the Cu–S bond is weak and the Cu vacancy and In substitute are preferably generated. Therefore, it is reasonable to increase the fluorescence intensity by the introduction of Cu defect which can be realized by decreasing the Cu content in the raw material solution. Fig.7b demonstrates that, as the Cu content getting poorer, the maximum QY% reaches from 0.84% to 6.90%, which implies the plenitude of Cu defect inducing the increase of fluorescent intensity. Hence, the grain size and QY% can be tuned by altering the In/Cu molar ratio, effectively.

The influence of surface ligand

The nanoparticles with high surface energy tend to be unstable and easily aggregate unless with the help of surface ligand. Previous works[49-50] reported that surface ligand could be used in controlling the fluorescence properties and morphology by altering the kind or volume of surface ligand. Among them, various ligands have been used e.g. DDT, mercaptopropionic

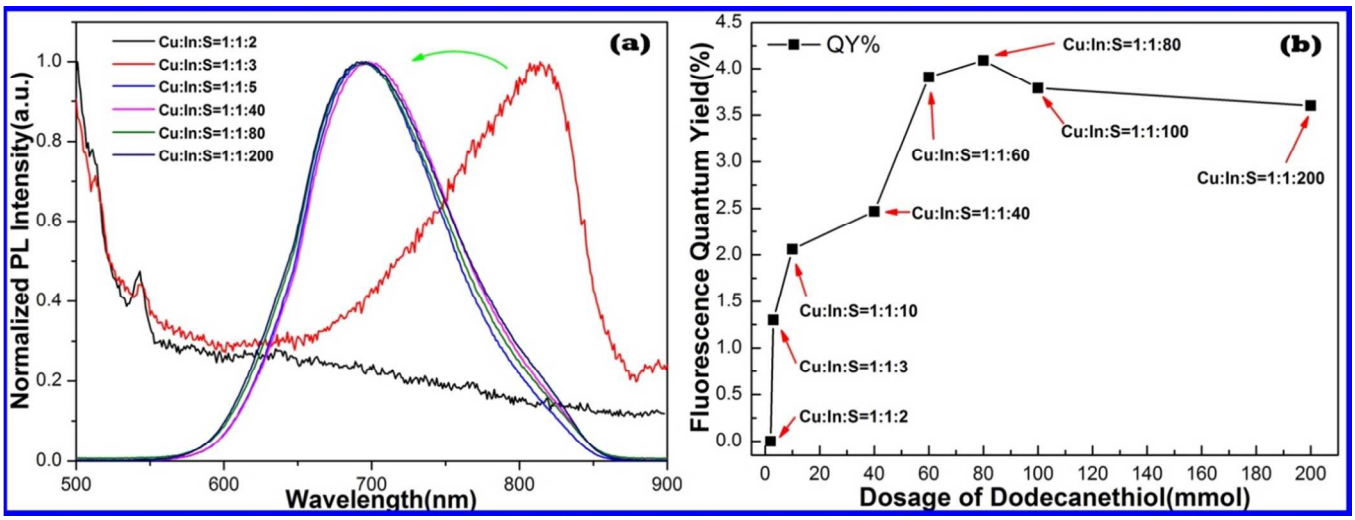

Fig. 8 (a) PL spectra of CIS QDs sampling at 20minwith different dosage of DDT at 230℃. (b) The maximum QY% of CIS QDs with different dosage of DDT at 230℃.

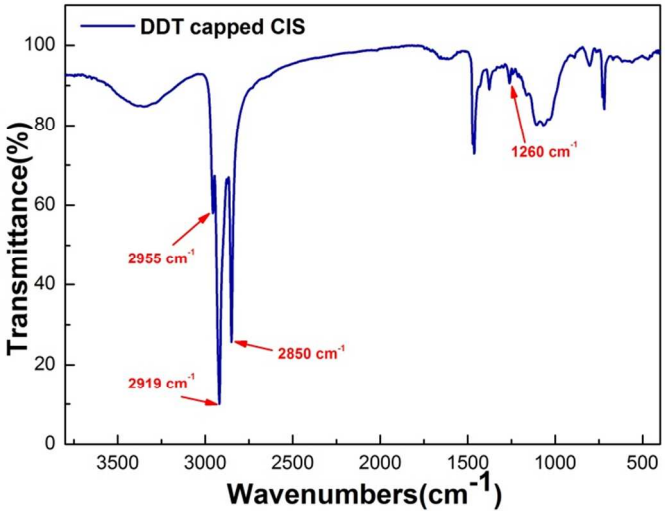

Fig. 9 IR spectra of CIS QDs sampling at 20min at 230℃

acid (MPA), oleylamine (OA), tri-n-octylphosphine (TOP), trioctylphosphine (TOPO), triphenylphosphine (TBP).[51-52]

In our study, we selected DDT both as sulfur source and surface ligand, which reduced the consumption of raw materials, substantially. With the purpose of confirming the assumption, IR (fig.9) was taken to verifying the actual surface ligand. A weak absorption located at 1260 cm^{-1} is indentified from the IR spectra, which is possible ascribed to the CH_2-S- wagging vibration. Three distinct absorption peaks around 2900 cm^{-1} are assigned to CH_3 asymmetric stretching, CH_2 asymmetric stretching and CH_2 symmetric stretching, respectively. Hence, it can be affirmed that the surface ligand is DDT.

Here, we studied the influence of different dosages of DDT on the optical properties of CIS QDs. The amount of DDT was calculated by molar ratio X= n_s/n_{cu} (keeping n_{In}/n_{Cu}=1). In the fig. 8a, a distinct blue shift is observed with a slight increase of X from 3 to 5 and that is too small when X kept rising. This phenomenon suggests that when the dosage of DDT is added in line with stoichiometric ratio (X=2) or lower, the ultra-small particles will aggregate into bulk status owning to the lack of surface stabilizers and surface ligand is adequate enough to maintain the stability of nanocrystals with the increase of X whose value exceed 5. The changes indirectly confirm DDT acting as surface ligand in keeping with results of IR.

As can be seen from the fig. 8b, the maximum QY% of CIS QDs can be tuned by manipulating additive amount of surface ligand, namely DDT. When X is 2 or lower, the value of QY% tends to be zero and the raw products easily turn into black precipitation, which implies that the sample prepared are unstable. Subsequently, the QY% see an upward trend ($2 \leqslant X \leqslant 80$) and reaches the highest point (X=80) followed by a slight decrease ($X \geqslant 80$) after adding excessive DDT. It is quite clear that the QY% is restricted if it is short of DDT. However, overabundance of surface ligand is still not beneficial to the enhancement of fluorescent intensity. To the best of our knowledge, DDT is Lewis base that preferably bonds to cationic sites on the surface. Along with the increase of DDT, the steric hindrance, which imposes on the neighbor surface sites, gradually strengthens caused by the long carbon chain. This leads to incomplete electronic passivation of surface dangling orbitals. The presence of such sites provides efficient pathways for non-radiative decay of nanocrystals excited state, which limits the maximum QY%. That is why the maximum QY% decreases after adding excessive DDT. Here, we choose X=80 as the ideal proportion because of the highest QY%. Meanwhile, in order to figure out the fluorescent stability of CIS QDs, we adopted this ideal ligand proportion mentioned above and tested the fluorescent intensity of samples extracted at the first 20min with the extension of keeping time at room temperature for 30 days. The final fluorescent intensity accounts for about 80% of the initial figures, which demonstrats the excellent fluorescent stability of CIS QDs prepared by one-pot method.

Conclusions

In summary, a simple and straightforward approach i.e. one-pot method was directly introduced to synthesize remarkable stable and monodispersity bare CIS QDs with outstanding photoluminescence ability ranging from 630 to 825 nm at 230℃. The maximum QY% could reach around 7% by making good use of crystal defects and the particle size can be tuned from 1.5 to 4 nm by adjusting In/Cu molar ratio. Additionally, the possible growth kinetics and formation mechanism of CIS QDs were analyzed and inferred, which paves a solid foundation for the future synthesis of Ⅰ-Ⅲ-Ⅵ QDs. Theoretically, this environmental friendly and near-infrared emission nanoparticle will be a promising alternative applied to the fluorescence bio-imaging in vivo after proper surface modification.

Acknowledgements

The work was partially supported by the National Natural Science Foundation of China (nos. 51172218) and the China Postdoctoral Science Foundation funded project (2013M541962).

Notes and references

The calculation of E_g can be found in supplementary information

[a] College of Chemistry and Chemical Engineering, Ocean University of China

[b] Institute of Material Science and Engineering, Ocean University of China

* Corresponding author information: caolixin@ouc.edu.cn

1 G. Mandal, M. Darragh, Y. A. Wang and C. D. Heyes, *Chem. Commun.* 2013, **49**, 624–626.
2 W. Guo, N. Chen, Y. Tu, C. Dong, B. Zhang, C. Hu and J. Chang, *Theranostics*, 2013, **3**, 99–108.
3 I. Gur, N. A. Fromer, M. L. Geier and A. P. Alivisatos, *Science*, 2005, **310**, 462–465.
4 P. V. Kamat, *J. Phys. Chem. C*, 2008, **112**, 18737–18753.
5 L. Yi, Y. Liu, N. Yang, Z. Tang, H. Zhao, G. Ma, Z. Sua and D. Wang, *Energy Environ. Sci.* 2013, **6**, 835–840.
6 A. L. Rogach, N. Gaponik, J. M. Lupton, C. Bertoni, D. E. Gallardo, S. Dunn, N. L. Pira, M. Paderi, P. Repetto, S. G. Romanov, C. O'Dwyer, C. M. S. Torres and A. Eychmüller, *Angew. Chem. Int. Ed.* 2008, **47**, 6538–6549.
7 W. S. Song, J. H. Kim, J. H. Lee, H. S. Lee, Y. R. Dob and H. Yang, *J. Mater. Chem.* 2012, **22**, 21901–21908.
8 S. Kim, B. Fisher, H. J. Eisler and M. Bawendi, *J. Am. Chem. Soc.* 2003, **125**, 11466–11467.
9 L. S Li, N. Pradhan, Y. Wang and X. Peng, *Nano Lett.* 2004, **4**, 2261–2264.
10 W. Jiang, A. Singhal, J. Zheng, C. Wang and W. C. W. Chan, *Chem. Mater.* 2006, **18**, 4845−4854.
11 D. Battaglia and X. Peng, *Nano Lett.* 2002, **2**, 1027−1030.
12 S. Debnath, R. Cherian and P. Mahadevan, *J. Phys. Chem. C*, 2013, **117**, 21981−21987.
13 M. A. Hines and G. D. Scholes, *Adv. Mater.* 2003, **15**, 1844−1849.
14 K. R. Choudhury, Y. Sahoo, T. Y. Ohulchanskyy and P. N. Prasad, *Appl. Phys. Lett.* 2009, **87**, 073110–073110-3.
15 L. Li, A. Pandey, D. J. Werder, B. P. Khanal, J. M. Pietryga and V. I. Klimov, *J. Am. Chem. Soc.* 2011, **133**, 1176-1179.
16 W. C. Huang, C. H. Tseng, S. H. Chang, H. Y. Tuan, C. C. Chiang, L. M. Lyu and M. H. Huang, *Langmuir,* 2012, **28**, 8496−8501.
17 E. Witt and J. Kolny-Olesiak, *Chem. Eur. J.* 2013, **19**, 9746−9753.
18 R. Xie, M. Rutherford and X. Peng, *J. Am. Chem. Soc.* 2009, **131**, 5691–5697.
19 J. K Oh, *J. Mater. Chem.* 2010, **20**, 8433–8445.
20 J. L. Blackburn, H. Chappell, J. M. Luther, A. J. Nozik and J. C. Johnson, *J. Phys. Chem. Lett.* 2011, **2**, 599–603.
21 R. Klenk, U. Blieske, V. Dieterle, K. Ellmer, S. Fiechter, I. Hengel, A. JagerWaldau, T. Kampschulte, C. Kaufmann, J. Klaer, M. LuxSteiner, D. Braunger, D. Hariskos, M. Ruckh and H. W. Schock, *Sol. Energ. Mat. Sol. C*, 1997, **49**, 349–356.
22 S. L. Castro, S. G. Bailey, R. P. Raffaelle, K. K. Banger and A. F. Hepp, *Chem. Mater.* 2003, **15**, 3142–3147.
23 R. E. Bailey and S. Nie, J. Am. Chem. Soc. 2003, **125**, 7100–7106.
24 W. Jiang, E. Papa, H. Fischer, S. Mardyani and W. C. W. Chan, *Trends in Biotechnol.* 2004, **22**, 607–609.
25 S. L. Castro, S. G. Bailey, R. P. Raffaelle, K. K. Banger and A. F. Hepp, *J. Phys. Chem. B*, 2004, **108**, 12429–12435.
26 J. J. Nairn, P. J. Shapiro, B. Twamley, T. Pounds, R. V. Wandruszka, T. R. Fletcher, M. Williams, C. Wang and M. G. Norton, *Nano Lett.* 2006, **6**, 1218–1223.
27 M. A. Malik, P. O'Brien and N. Revaprasadu, *Adv. Mater.* 1999, **11**, 1441–1444.
28 M. G. Panthani, V. Akhavan, B. Goodfellow, J. P. Schmidtke, L. Dunn, A. Dodabalapur, P.F. Barbara and B. A. Korgel, *J. Am. Chem. Soc.* 2008, **130**, 16770–16777.
29 B. Li, Y. Xie, J. Huang and Y. Qian, *Adv. Mater.* 1999, **11**, 1456–1459.
30 Q. Lu, J. Hu, K. Tang, Y. Qian, G. Zhou and X. Liu, *Inorg. Chem.* 2000, **39**, 1606–1607.
31 H. Nakamura, W. Kato, M. Uehara, K. Nose, T. Omata, S. Otsuka-Yao-Matsuo, M. Miyazaki and H. Maeda, *Chem. Mater.* 2006, **18**, 3330–3335.
32 L. Li, T. J. Daou, I. Texier, T. T. K. Chi, N. Q. Liem and P. Reiss, *Chem. Mater.* 2009, **21**, 2422–2429.
33 H. Zhong, S. S. Lo, T. Mirkovic, Y. Li, Y. Ding, Y. Li and G. D. Scholes, *ACS Nano*, 2010, **4**, 5253–5262.
34 I. V. Bodnar, *Inorg. Mater.* 2000, **36**, 108–110.
35 K. Nose, Y. Soma, T. Omata and S. Otsuka-Yao-Matsuo, *Chem. Mater.* 2009, **21**, 2607–2613.
36 D. C. Pan, L. J. An, Z. M. Sun, W. Hou, Y. Yang, Z. Z. Yang and Y. F. Lu, *J. Am. Chem. Soc.* 2008, **130**, 5620–5621.
37 S. H. Lee, *Electron. Mater. Lett.* 2012, **8**, 191–197.
38 L. E. Brus, *J. Chem. Phys.* 1984, **80**, 4403–4409.
39 H. Zhong, Y. Zhou, M. Ye, Y. He, J. Ye, C. He, C. Yang and Y. Li, *Chem. Mater.* 2008, **20**, 6434–6443.
40 X. Wang, D. Pan, D. Weng, C. Y. Low, L. Rice, J. Han and Y. Lu, *J. Phys. Chem. C*, 2010, **114**, 17293–17297.
41 D. E. Nam, W. S. Song and H. Yang, *J. Colloid Interf. Sci.* 2011, **361**, 491–496.
42 M. Kruszynska, H. Borchert, J. Parisi and J. Kolny-Olesiak, *J. Am. Chem. Soc.* 2010, **132**, 15976–15986.
43 S. T. Connor, C. Hsu, B. D. Weil, S. Aloni and Y. Cui, *J. Am. Chem. Soc.* 2009, **131**, 4962–4966.
44 M. Ahmadi, S. S. Pramana, L. Xi, C. Boothroyd, Y. M. Lam and S. Mhaisalkar, *J. Phys. Chem. C*, 2012, **116**, 8202−8209.
45 S. L. Castro, S. G. Bailey, R. P. Raffaelle, K. K. Banger, A. F. Hepp. J. Phys. Chem. B 2004, 108, 12429-12435.
46 H. Nakamura, W. Kato, M. Uehara, K. Nose, T. Omata, S. Otsuka-Yao-Matsuo, M. Miyazaki, H. Maeda, Chem. Mater. 2006, 18, 3330-3335.
47 J. S. Gardner, E. Shurdha, C. Wang, L. D. Lau, R. G. Rodriguez, J. J. Pak, J. Nanopart. Res. 2008, 10, 633–641.
48 M. Uehara, K. Watanabe, Y. Tajiri, H. Nakamura, H. Maeda, J. Chem. Phys. 2008,129, 134709:1-6.
49 Z. Liu, L. Wang, Q. Hao, D. Wang, K. Tang, M. Zuo, Q. Yang, CrysEngComm. 2013, 15, 7192-7198
50 J. He, W. Zhou, J. Guo, M. Li, S. Wu, CrysEngComm. 2012, 14, 3638-3644
51 W. W. Yu, Y. A. Wang and X. Peng, Chem. Mater. 2003, 15, 4300–4308.
52 X. Jin, J. Parisi and J. Kolny-Olesiak, J. Nanopart. Res. 2013, 243831:1-7.

